Modeling Cable-Suspended Multidrone Manipulation Using Grasping Theory

Modeling Cable-Suspended Multidrone Manipulation Using Grasping Theory

Giovanni Cortigiani, Yaolei Shen, Maria Pozzi, *Member, IEEE*, Chiara Gabellieri, *Member, IEEE*, Monica Malvezzi, Antonio Franchi, *Fellow, IEEE*, and Domenico Prattichizzo, *Fellow, IEEE*

***Abstract*—The mechanical principles regulating grasping and manipulation with multifingered robotic hands have been widely studied in the literature, leading to a well-established theoretical framework. In this article, we show that, under certain hypotheses, these findings can be applied to the case of cable-suspended aerial multidrone manipulation, where the contacts between the robots and the object are mediated by cables. The devised unified and versatile mathematical framework is validated through numerical simulations and real-world experiments in static and free flight conditions, showing that it can be exploited for accurately describing the properties of different configurations of drones and cables. The new insights illustrated in this work allow to transfer the current results devised in the field of robotic grasping—and potentially the future ones—to the field of cable-suspended multidrone manipulation.**

***Index Terms*—Grasping and manipulation, unmanned autonomous systems.**

I. Introduction

The problem of grasping and manipulating objects with robots has been investigated from the early stages of robotics research [1], and the mathematical model of robotic grasping [2], [3] has setup the bases for grasp analysis and grasp synthesis with multifingered hands. The framework summarized in [2] is general enough to be extended to account for new elements, including passive compliance and underactuation in the hand structure [4], exploitation of environmental constraints [5], and teams of cooperative robots [6].

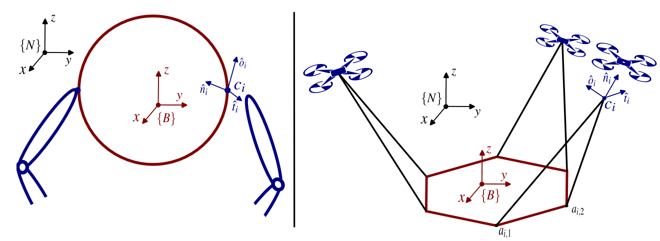

Fig. 1. Grasp modeling applied to two different systems. The robotic fingers (left) directly apply forces on the object at the contact points [2], whereas the drones (right) hold the object, thanks to cables [7]. $\{\mathbf{N}\}$, $\{\mathbf{B}\}$, and $\{\mathbf{C}\}_i$ indicate the frames of the world, the object, and the ith contact point, respectively.

In this article, we show that the well-known grasp model for multifingered hands detailed in [2] can also be extended to derive the structural properties and the force transmission model of *cable-suspended multidrone manipulation systems* consisting of small aerial vehicles steering together a cable-suspended platform.

The two manipulation systems considered in this work are sketched in Fig. 1. While the robotic hand directly applies forces on the object through unilateral contact constraints between its fingers and the object, in the cable-suspended manipulation system the contact between the drones and the object is guaranteed by cables. This fact translates into different constraints that must be satisfied in order for the grasp to hold. With finger contacts the grasp is maintained by pushing the object, whereas with cables the grasp is maintained by pulling it. To avoid slippage at the contacts, the forces applied by the fingers of a robotic hand must lie inside the "Friction Cone," under the hypotheses of coulomb friction constraints [2]. For the cable suspended manipulation system, instead, the force exerted by each drone has to lie in a space delimited by the prolongation of the cables. This is crucial to avoid the slackening of cables.

While the analogy between grasping with multifingered hands, parallel manipulators, and cable-driven robots has already been tackled in the literature [8], [9], to the best of the authors' knowledge, this is the first time in which a precise

Received 3 February 2026; revised 1 April 2026; accepted 12 May 2026. Recommended by Technical Editor Z. Chen and Senior Editor H. Wang. This work was supported by the European Union by the Next Generation EU project ECS17 "THE - Tuscany Health Ecosystem" (PNRR MUR M4 C2 Inv. 1.5, CUP B63C22000680007, Spoke 9: Robotics and Automation for Health), in part by the Leonardo S.p.A. under Grant LDO/CTI/P/0025793/22, and in part by the Horizon Europe research under Grant 101120732 (AUTOASSESS). *(Corresponding author: Giovanni Cortigiani.)*

Giovanni Cortigiani, Maria Pozzi, and Domenico Prattichizzo are with the Department of Information Engineering and Mathematics, University of Siena, 53100 Siena, Italy, and also with the Humanoids and Human Centered Mechatronics, Istituto Italiano di Tecnologia, 16163 Genoa, Italy (e-mail: giovann.cortigiani@student.unisi.it).

Yaolei Shen and Chiara Gabellieri are with the Robotics and Mechatronics Department, University of Twente, 7500 AE Enschede, The Netherlands.

Monica Malvezzi is with the Department of Information Engineering and Mathematics, University of Siena, 53100 Siena, Italy.

Antonio Franchi is with the Robotics and Mechatronics Department, University of Twente, 7500 AE Enschede, The Netherlands, and also with the Department of Computer, Control and Management Engineering, Sapienza University of Rome, 00185 Roma, Italy (e-mail: schol@r-franchi.eu).

This article has supplementary material provided by the authors and color versions of one or more figures available at https://doi.org/10.1109/TMECH.2026.3694490.

Digital Object Identifier 10.1109/TMECH.2026.3694490

and formalized connection between grasp modeling in multifingered hands and cable-suspended multidrone manipulation is presented. Building on this analogy, we develop a novel grasp model for cable-suspended manipulation that describes how forces generated by multiple drones are transmitted to a payload through cables. Differently from what is typically done in the aerial cooperative manipulation of cable-suspended objects [10], [11], this work takes a step further by modeling the contact points at the drone attachment points instead of at the object. This enables to directly define the forces transmitted from each drone to the object, as well as the drone's actuation limits and the cables tautness constraints, accounting for a generic number of cables per drone, exploiting the analogy with the friction cone. In addition, we also derive the structural properties of the system, and the resulting grasp wrench space under cable constraints.

The validity of the proposed model is demonstrated through numerical analyses and real-world experiments involving different configurations of drones and cables, both in static conditions and during free-flight manipulation.

The key advancement of this article lies in the fact that the proposed approach provides a general formalism that allows applying the results from the theory of multifingered grasping to the emerging field of cable-suspended manipulation by drones. Within this framework, established tools from grasping, such as grasp quality metrics, force optimization algorithms, and grasp synthesis methods, can be directly applied to multidrone systems. As an example, the Supplementary Material of this article illustrates the application of the proposed model to optimize the drones' individual thrust across different system configurations, while minimizing the total thrust usage and/or the likelihood of slackening the cables (see Section S.1 of the Supplementary Material).

II. Related Works

The kineto-static analysis of a multifingered hand grasping an object is akin to that of other closed-chain systems [12], including collaborative manipulators [13], parallel manipulators [9], [14], and cable-driven parallel robots (CDPRs) [8]. Borras and Dollar [9], [15] showed the equivalence between the kineto-static equations of parallel manipulators and those of multifingered robotic hands, applying it to study the workspace of an underactuated gripper. Similarly, Özgür et al. [14] analyzed the dexterity of grasping mechanisms using the theoretical framework of parallel manipulation. Ebert-Uphoff and Voglewede [8] analyzed for the first time the modeling similarities between grasping and CDPRs in the planar case. However, the concept of friction cone is applied to CDPRs only for the planar derivation of force closure conditions, and not to define mathematical constraints on the transmitted contact forces, as each cable is actuated by its own motor. In subsequent studies, the antipodal grasp theorem and force closure conditions were derived for planar CDPRs [16], and methods to compute the wrench feasible workspace and exploit it in planning tasks with 3-D CDPRs were proposed [17], [18].

The use of cables instead of rigid links in manipulation systems gives many advantages, including a much larger workspace and intrinsic compliance [19]. Thus, in recent years, tethered connections have been widely adopted in the field of cooperative aerial manipulation [20], [21], [22]. Compared to the adoption of ad hoc manipulators attached to the drones, cables are lightweight and provide decoupling between the attitude of the robots and the dynamics of the system [10]. The problem of controlling the drones to maintain the equilibrium of the cable-suspended payload has been widely studied [23], [24], [25], also considering the robustness to external disturbances [7].

The structural similarities between multidrone cable suspended manipulation and CDPRs were exploited for planning the motion of multidrone systems in [11] and [26]. However, while both CDPRs and multidrone cable-suspended systems transmit forces through cables, their mechanics differ significantly: in multidrone manipulation, more cables can be attached to the same drone (coupled tensions) and the object is moved by repositioning the drones rather than by directly controlling cable lengths as in CDPRs [18]. Thus, grasping theory provides a more direct and natural framework for describing the forces and motions transmitted through the cables from the drones to the object, just like they are transmitted through the contacts from the fingers to the object. Manubens et al. [11] proposed a quasi-static motion planning approach for a simulated system of three drones and six fixed-length cables called the "Fly-Crane,"using the cables tensions constraints derived for CDPRs. However, the derived cable tension constraints consider each cable separately, and the kinematics and the thrust constraints are derived for the specific configuration of cables and drones taken into account in this article. Moreover, the analysis does not consider the dynamics of the system. Masone et al. [26] proposed to use the conventional model of reconfigurable cable-driven parallel robots (RCDPRs) to derive an explicit mathematical relation between the motion of the quadrotors and the motion of the payload, so that the internal motions of the system can be exploited to perform secondary tasks. The dynamics of the system is considered, but still the analogy with RCDPRs only allows for considering one cable per drone. In addition, both [11] and [26] did not apply their approach in real-world experiments, but only in simulation.

As underlined in this literature review, several works have exploited the kineto-static similarities among different robotic systems to apply results across different domains: from parallel robots to grasp analysis [9], from grasp analysis to CDPRs [8], and from CDPRs to cable-suspended multidrone manipulation [11]. However, what was still missing was a precise and formalized connection between grasp modeling in multifingered hands and cable-suspended multidrone manipulation. To fill this gap, this work proposes a novel formulation that explicitly establishes this analogy.

III. Methodology

In this section, first the main equations and properties of the grasp model for cable-suspended manipulation are presented (see Sections III-A and B), and, based on those, the constraints to be satisfied to keep the cables taut are formulated (see Section III-C). The adopted notation is based on [2] and is outlined in Table I.

This article has been accepted for inclusion in a future issue of this journal. Content is final as presented, with the exception of pagination.

TABLE I
NOTATIONS FOR THE TWO MODELS

Notation	Multi-fingered Hands	Cable-suspended Multi-Drone Systems
$\{\mathbf{N}\}$	World Reference Frame	World Reference Frame
$\{\mathbf{B}\}$	Object Reference Frame	Object Reference Frame
$\mathbf{c}_i \in \mathbb{R}^3$	Position of Contact Point i w.r.t. $\{\mathbf{N}\}$	Position of Drone Attachment Point i w.r.t. $\{\mathbf{N}\}$
$\{\mathbf{C}\}_i = \{\hat{\mathbf{n}}_i, \hat{\mathbf{t}}_i, \hat{\mathbf{o}}_i\}$	Contact Reference Frame	Drone Attachment Point Reference Frame
n_d	Number of Contacts	Number of Drones
n_{c_i}	-	Number of Cables attached to drone i
$\mathbf{a}_{ij}$	-	Object anchor point of cable j connected to drone i
$\boldsymbol{\lambda} \in \mathbb{R}^{n_\lambda}$	Contact Wrench Components w.r.t. $\{\mathbf{C}\}_i$	Wrench Components transmitted by the Drones w.r.t. $\{\mathbf{C}\}_i$
n_λ	Number of transmitted Contact Wrench Components	Number of transmitted Drone Wrench Components
$\mathbf{H} \in \mathbb{R}^{n_\lambda \times 6n_d}$	Transmitted Contact Wrenches Selection Matrix	Transmitted Drone Forces Selection Matrix

A. Grasp Model for Cable-Suspended Multidrone Manipulation

Referring to the left side of Fig. 1, the frame $\{\mathbf{N}\}$ represents the world reference frame, while the frame $\{\mathbf{B}\}$ indicates the reference frame fixed to the object, having the origin in the center of mass of the object. The vector $\mathbf{p} \in \mathbb{R}^3$ represents the position of $\{\mathbf{B}\}$ with respect to (w.r.t) $\{\mathbf{N}\}$. Let the frame $\{\mathbf{C}\}_i = \{\hat{\mathbf{n}}_i, \hat{\mathbf{t}}_i, \hat{\mathbf{o}}_i\}$ define the reference frame of the ith contact point. The unit vector $\hat{\mathbf{n}}_i$ is oriented toward the object, normal to the contact tangent plane. The other two unit vectors are orthogonal to $\hat{\mathbf{n}}_i$ and lie in the tangent plane of the contact. The position of contact point i in $\{\mathbf{N}\}$ is represented by the vector $\mathbf{c}_i \in \mathbb{R}^3$.

Let $\boldsymbol{\lambda}$ represent the vector consisting of contact force and moment components transmitted through the contacts and expressed in the contact frames. In particular, $\lambda = [\lambda_1^{\mathrm{T}} \cdots \lambda_{n_d}^{\mathrm{T}}]^{\mathrm{T}} \in \mathbb{R}^{n_\lambda}$, where each λ_i is expressed in the contact frame $\{\mathbf{C}\}_i$, n_d is the number of contact points, and n_λ is the total number of force and moment components transmitted at the contacts. Defining $\mathbf{g} \in \mathbb{R}^6$ as the external wrench applied to the object by noncontact forces [2], expressed in the reference frame $\{\mathbf{N}\}$, the object equilibrium equations can be written as

$$\mathbf{g} = -\mathbf{G}\lambda \tag{1}$$

where $\mathbf{G} \in \mathbb{R}^{6\times n_\lambda}$ is the *Grasp Matrix*. The Grasp Matrix is obtained as $\mathbf{G} = \tilde{\mathbf{G}}\mathbf{H}^{\mathrm{T}}$, where $\tilde{\mathbf{G}} \in \mathbb{R}^{6\times 6n_d}$ is the *Complete Grasp Matrix*, computed as $\tilde{\mathbf{G}} = [\tilde{\mathbf{G}}_1 \cdots \tilde{\mathbf{G}}_{n_d}]$, with

$$\tilde{\mathbf{G}}_i = \begin{bmatrix} \mathbf{R}_{\mathbf{C}_i}^{\mathbf{N}} & \mathbf{0} \\ \mathbf{S}(\mathbf{c}_i - \mathbf{p})\mathbf{R}_{\mathbf{C}_i}^{\mathbf{N}} & \mathbf{R}_{\mathbf{C}_i}^{\mathbf{N}} \end{bmatrix} \tag{2}$$

where $\mathbf{R}_{\mathbf{C}_i}^{\mathbf{N}}$ is the orientation of the ith contact frame $\{\mathbf{C}\}_i$ w.r.t $\{\mathbf{N}\}$, and $\mathbf{S}(\cdot)$ is the cross product matrix. $\mathbf{H} \in \mathbb{R}^{n_\lambda \times 6n_d}$ is the *Selection Matrix*, which selects which force and moment components are transmitted to the object through the contacts according to the considered contact model. According to [2], contact models mostly adopted in grasping analysis can be classified into three main types: *Point Contact without Friction*, where only the normal component of the force is transmitted; *Hard Finger*, where the three components of the force are transmitted; *Soft Finger*, where also the normal component of the moment is selected. More details on the computation of the Grasp Matrix can be found in [2].

From the kinematics point of view, $\mathbf{G}^{\mathrm{T}}$ maps the twist of the object (ν) to the transmitted contact twists (ν_{cc})

$$\nu_{cc} = \mathbf{G}^{\mathrm{T}}\nu. \tag{3}$$

In the case of cable-suspended manipulation, referring to the right part of Fig. 1, we define as *Drone Attachment Point* $\mathbf{c}_i$ the point on the drone i to which the cables are attached. In this model, we assume the cables to be nonextendable. At $\mathbf{c}_i$, we define a frame $\{\mathbf{C}\}_i$, with axes $\{\hat{\mathbf{n}}_i, \hat{\mathbf{t}}_i, \hat{\mathbf{o}}_i\}$. We define as *Object Anchor Points* the points where the cables are anchored to the object. Namely, $\mathbf{a}_{ij}$ is the point in which the cable j of drone i is anchored to the object. The vector $\boldsymbol{\lambda}$ represents the forces transmitted by the drones to the object through the cables, whereas again with $\mathbf{g} \in \mathbb{R}^6$ we indicate the noncontact object wrench expressed in the reference frame $\{\mathbf{N}\}$.

A. Force transmission: In the cable-suspended grasp model, the Selection Matrix $\mathbf{H}$ selects the force and moment components applied by the drones that are transmitted to the object through the cables. Let n_{c_i} indicate the number of cables attached to the drone i, and n_{λ_i} indicate the number of force components transmitted by drone i. The Selection Matrix $\mathbf{H}_i \in \mathbb{R}^{n_{\lambda_i}\times 6}$ for each drone i is defined as

$$\mathbf{H}_i = \left[\mathbf{H}_{iF} \;\middle|\; \mathbf{0}_{n_{\lambda_i}\times 3}\right] \tag{4}$$

where $\mathbf{H}_{iF} \in \mathbb{R}^{n_{\lambda_i}\times 3}$ is the translational component of the Selection Matrix. Notice that the rotational component of the Selection Matrix is always null, since there is no possibility of transmitting any moment. The overall Selection Matrix $\mathbf{H}$ is given by: $\mathbf{H} = \mathrm{Blockdiag}(\mathbf{H}_1, \ldots, \mathbf{H}_{n_d}) \in \mathbb{R}^{n_\lambda \times 6n_d}$.

As long as $n_{c_i} \leq 3$, the number of cables attached to each drone directly reflects the number of force components that the drone is able to apply to the object, i.e., $n_{\lambda_i} = n_{c_i}$. If this is valid for each drone i, then $n_\lambda = n_c$, where $n_c = \sum_{i=1}^{n_d} n_{c_i}$ is the total number of cables in the system. For $n_{c_i} = 1$, we choose the reference frame of the drone attachment point with the normal component $\hat{\mathbf{n}}_i$ aligned with the cable. For $n_{c_i} = 2$, we assume that the contact reference frame with the $\hat{\mathbf{n}}_i$ and $\hat{\mathbf{t}}_i$ components lying on the plane described by the two cables, and the other component $\hat{\mathbf{o}}_i$ orthogonal to them as shown in Fig. 1. For $n_{c_i} = 3$, the three cables should not be collinear, and the reference frame can be chosen arbitrarily. Then, the matrices $\mathbf{H}_{iF}$ for

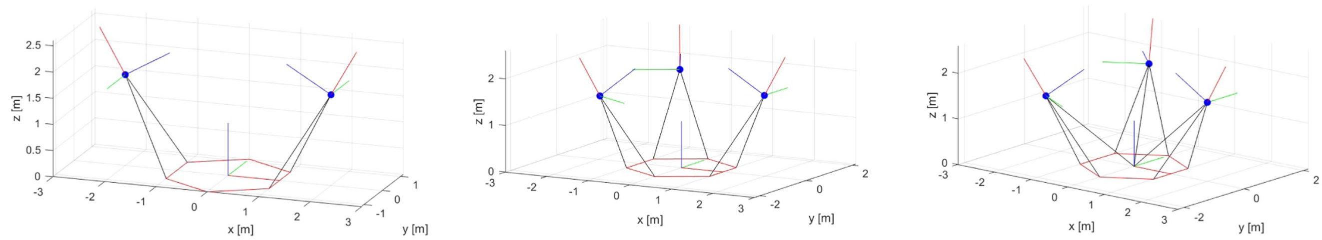

(a) (b) (c)

Fig. 2. Representative Examples. The red hexagon is the object to be manipulated, the blue dots are the drone attachment points, while the black lines are the cables. The reference frames of object and drone attachment points are depicted with RGB triplets. (a) 2 drones and 4 cables; (b) 3 drones and 6 cables; (c) 3 drones and 9 cables.

$n_{c_i} = 1$, $n_{c_i} = 2$, and $n_{c_i} = 3$, are, respectively

$$\mathbf{H}_{iF} = \begin{bmatrix} 1 & 0 & 0 \end{bmatrix}, \mathbf{H}_{iF} = \begin{bmatrix} 1 & 0 & 0 \\ 0 & 1 & 0 \end{bmatrix}, \mathbf{H}_{iF} = I_{3\times 3}. \quad (5)$$

According to the new definitions related to the case of cable-suspended manipulation, (1) can now be used to express how the forces that the drones apply through the cables are transmitted to the object, and (3) can be used to describe the kinematic relation between the twist of the object and the twists transmitted at the drones attachment points.

B. Structural Properties of Cable-Suspended Grasps

When manipulating an object, the main *structural properties* to take into account are 1) the set of object wrenches that the drones are not able to resist, and 2) the conditions under which any object wrench can be resisted. In the case of multifingered hands, these properties can be analyzed by considering the null spaces $\mathcal{N}(\cdot)$ of $\mathbf{G}$ and $\mathbf{G}^{\mathrm{T}}$, as shown in [2]. The same reasoning outlined in [2] can be applied to the case of cable suspended manipulation, deriving the following properties of the system.

Graspability: Analysing (1), it can be derived that if $\mathcal{N}(\mathbf{G}) \neq \{\mathbf{0}\}$ (i.e., $\mathcal{N}(\mathbf{G})$ is nontrivial), $\exists \lambda \neq \mathbf{0} \,|\, \mathbf{G}\lambda = \mathbf{0}$. In other words, the transmitted wrenches $\lambda \in \mathcal{N}(\mathbf{G})$ do not apply any wrench on the object. If $\mathcal{N}(\mathbf{G})$ is nontrivial, then the system is said to be *graspable*. For multifingered hands, vectors in $\mathcal{N}(\mathbf{G})$ are called *internal forces* and they play a key role in holding an object, as they affect the tightness of the grasp [27]. By spanning $\mathcal{N}(\mathbf{G})$, it is possible to optimally choose the contact forces according to specific objectives [4]. A similar approach can be adopted in cable-suspended multidrone systems to find optimal drone forces that satisfy tautness constraints and allow to resist/generate a given object wrench.

Indetermination: Let us consider (3). If $\mathcal{N}(\mathbf{G}^{\mathrm{T}}) \neq \{\mathbf{0}\}$ it means that $\exists \nu \neq \mathbf{0} \,|\, \mathbf{G}^{\mathrm{T}}\nu = \mathbf{0}$. In other words, the object twists $\boldsymbol{\nu} \in \mathcal{N}(\mathbf{G}^{\mathrm{T}})$ represent the motions of the object that do not affect the motion of the drone attachment points, and thus they cannot be controlled by drone motions. In this case, the system is said to be *indeterminate*. Analogously, vectors in $\mathcal{N}(\mathbf{G}^{\mathrm{T}})$ describe the object wrenches, which cannot be resisted by the forces applied by the drones. As a consequence, a desirable property for a grasp, irrespective of whether it is performed by a multifingered hand or by a multidrone system, is to have $\mathcal{N}(\mathbf{G}^{\mathrm{T}}) = \{\mathbf{0}\}$.

Depending on the task to be accomplished, one may hence choose the number of drones and the number of cables for each drone to be used in a configuration directly analyzing which wrenches can (and cannot) be resisted. Indeed, the total number of cables in the system affects the dimensions of the null spaces. In particular, a rigid object has six degrees of freedom. If the system has a number of cables lower than 6, then the system is indeterminate because $\mathcal{N}(\mathbf{G}^{\mathrm{T}})$ is nontrivial and spans nonzero wrenches that cannot be resisted. On the other hand, a necessary condition for the system to be graspable (i.e., nontrivial $\mathcal{N}(\mathbf{G})$) is that the number of cables is greater than 6.

Representative examples: In Fig. 2, three different representative configurations where multiple drones are manipulating a hexagonal platform are shown. Let us consider the case shown in Fig. 2(a), where two drones are linked to the platform through two cables each, with $n_c = 4$. In this case, by computing the vector bases of $\mathcal{N}(\mathbf{G})$ and $\mathcal{N}(\mathbf{G}^{\mathrm{T}})$, we obtain

$$\mathbf{N}(\mathbf{G}) = \mathbf{0}_{4\times 1}, \quad \mathbf{N}(\mathbf{G}^{\mathrm{T}}) = \begin{bmatrix} 0.87 & 0 \\ 0 & -0.87 \\ 0 & 0 \\ 0 & -0.5 \\ 0.5 & 0 \\ 0 & 0 \end{bmatrix}. \quad (6)$$

The rank of $\mathbf{N}(\mathbf{G}^{\mathrm{T}})$ is equal to 2 and corresponds to the dimension of $\mathcal{N}(\mathbf{G}^{\mathrm{T}})$, which defines the space of uncontrollable object wrenches. Let us now consider the configuration in Fig. 2(b). Here, $n_c = 6$, and both null spaces become trivial

$$\mathbf{N}(\mathbf{G}) = \mathbf{0}_{6\times 1}, \quad \mathbf{N}(\mathbf{G}^{\mathrm{T}}) = \mathbf{0}_{6\times 1}. \quad (7)$$

By adding a cable to each of the three drones, ensuring that the attachment points on the objects are noncollinear [see Fig. 2(c)], the total number of cables increases to $n_c = 9$. The corresponding bases of $\mathcal{N}(\mathbf{G})$ and $\mathcal{N}(\mathbf{G}^{\mathrm{T}})$ are

$$\mathbf{N}(\mathbf{G}) = \begin{bmatrix} 0.36 & -0.18 & 0.07 \\ -0.07 & -0.33 & -0.47 \\ -0.63 & 0.30 & -0.12 \\ 0.26 & 0.31 & 0.05 \\ 0.19 & -0.23 & 0.49 \\ -0.45 & -0.54 & -0.09 \\ 0.20 & 0.03 & -0.36 \\ -0.12 & 0.56 & -0.02 \\ -0.34 & -0.05 & 0.62 \end{bmatrix}, \quad \mathbf{N}(\mathbf{G}^{\mathrm{T}}) = \mathbf{0}_{6\times 1}. \quad (8)$$

As previously pointed out, in this case, the system is graspable and thus the null space of $\mathbf{G}$ can be spanned to find an optimal set of contact forces. At the same time, however, the positions of the drones relative to the object must remain fixed to prevent the cables from slackening.

So far, we have presented the structural properties of cable-suspended systems, which are valid under the assumption of taut cables. The constraints that the forces applied by the drones must meet to maintain the cables tautness and transmit the forces to the object are discussed in the next section.

C. Cables Constraints and Grasp Wrench Space

In grasping with multifingered hands, contact forces are subject to limits and constraints due to hand properties and friction properties. For instance, in the case of a Hard Finger contact model, such constraints can be modeled by the so-called Coulomb friction cone, whose axis is normal to the surfaces at the contact point and whose amplitude angle is the friction angle defined by Coulomb's law. It is worth noting that the constraints are not linear, and several algorithms have been developed to account for this [2], [27].

Similarly, when dealing with cable-suspended manipulation, we can define the *Cables Cone* as the portion of space contained among the extensions of the cables. It describes the subspace in which the transmitted forces must lie in order to keep the cables taut. Differently from the grasp model for multifingered hands, the constraints on the forces λ_i at each drone attachment point $\mathbf{c}_i$ described by the cables cone are linear. The dimension of the space defined by the cone changes according to the number of cables (see Fig. 3). In general, the cable constraints for drone i can be written as

$$\mathbf{M}_i \lambda_i \geq \mathbf{0} \quad (9)$$

where $\mathbf{M}_i = [\hat{\mathbf{m}}_{i,1}, \ldots, \hat{\mathbf{m}}_{i,n_{c_i}}]^{\mathrm{T}} \in \mathbb{R}^{n_{c_i} \times n_{c_i}}$, and the inequality is meant elementwise. The definition of the entries of $\mathbf{M}_i$ depends on the number of cables attached drone i.

If $n_{c_i} = 3$, let ${}^{C}\hat{\mathbf{b}}_{i,j} \in \mathbb{R}^3$ define the 3-D unit vector describing the jth edge of the region, corresponding to the extension of the cable anchored at drone i and attachment point $\mathbf{a}_{ij}$, expressed in the contact frame $\{\mathbf{C}\}_i$. Then, $\hat{\mathbf{m}}_{i,j} \in \mathbb{R}^3$ indicates the vector normal to the plane generated by ${}^{C}\hat{\mathbf{b}}_{i,j}$ and ${}^{C}\hat{\mathbf{b}}_{i,j+1}$, i.e., $\hat{\mathbf{m}}_{i,j} = {}^{C}\hat{\mathbf{b}}_{i,j} \times {}^{C}\hat{\mathbf{b}}_{i,j+1}$ (if $j = n_{c_i}$, then $j+1 = 1$). When the cables are 3, the drone forces must lie inside a pyramidal sector whose edges are defined by the extensions of the cables. In this case, all the components of the forces applied by the drones are transmitted to the object. However, to maintain all the three cables taut, the drone attachment point position must not change. If $n_{c_i} = 2$, let ${}^{\bar{C}}\hat{\mathbf{b}}_{i,j} \in \mathbb{R}^2$ define the 2-D unit vector describing the jth edge of the region, expressed in the frame $\{\bar{\mathbf{C}}\}_i = \{\hat{\mathbf{n}}_i, \hat{\mathbf{t}}_i\}$. Then, $\hat{\mathbf{m}}_{i,j} \in \mathbb{R}^2$ corresponds to the vector normal to ${}^{\bar{C}}\hat{\mathbf{b}}_{i,j}$ lying in the plane of the cables unit vectors, and the cables cone becomes a circular sector, as shown in Fig. 3. If $n_{c_i} = 1$, then $\mathbf{M}_i = 1$, and the only constraint is for the force to be positive.

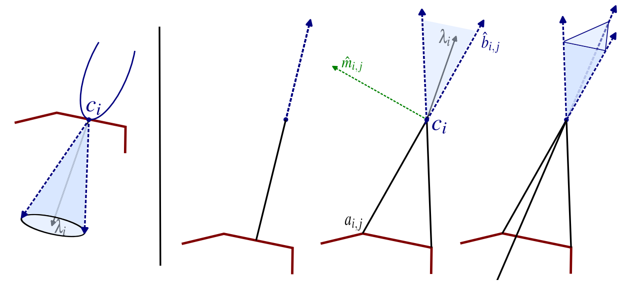

Fig. 3. Force constraints of the two different systems. On the left, the Coulomb Friction Cone used in the contact model with multifingered hands. On the right, the *Cables Cones* generated by different numbers of cables connecting the object to the drone, specifically $n_{c_i} = 1$, $n_{c_i} = 2$, and $n_{c_i} = 3$, respectively.

By defining $\mathbf{M} = \mathit{Blockdiag}(\mathbf{M}_1, \ldots, \mathbf{M}_{n_d})$, the cables constraints can be written in a compact form as

$$\mathbf{M}\lambda \geq \mathbf{0}. \quad (10)$$

Let us indicate with $\lambda'_{i,\max}$ the maximum thrust achievable by drone i, the following inequality must hold $\forall i = 1, \ldots, n_d$: $\|\lambda'_i\| \leq \lambda'_{i,\max}$, where λ'_i is the thrust applied by drone i defined as:

$$\lambda'_i = {}^{N}\lambda_i - m_i \mathbf{a}_g \quad (11)$$

where ${}^{N}\lambda_i$ is the transmitted drone force expressed in the world reference frame $\{\mathbf{N}\}$, m_i is the mass of drone i, and $\mathbf{a}_g$ is the gravitational acceleration. Let ${}^{N}\hat{\mathbf{b}}_{ij}$ be the unit vector of the jth cable connected to the drone i expressed in $\{\mathbf{N}\}$. Hence, the force applicable by drone i, expressed in $\{\mathbf{N}\}$, can be computed as the weighted sum of the unit vectors of the cables attached to drone i

$${}^{N}\lambda_i = \sum_{j=1}^{n_{c_i}} \sigma_{i,j}\, {}^{N}\hat{\mathbf{b}}_{ij}, \quad \|\lambda'_i\| \leq \lambda'_{i,\max}. \quad (12)$$

By indicating with $\mathbf{w}_{ij}$ the wrench that drone i can apply to the object through cable j, given by

$$\mathbf{w}_{ij} = \begin{bmatrix} {}^{N}\hat{\mathbf{b}}_{ij} \\ (\mathbf{c}_i - \mathbf{p}) \times {}^{N}\hat{\mathbf{b}}_{ij} \end{bmatrix} \quad (13)$$

the Grasp Wrench Space $\mathcal{W}$, describing all the possible wrenches $\mathbf{w}$ that the drones can apply to the object, can be defined as the Minkowski sum of the sets of wrenches $\mathbf{w}_i$ that can be generated

This article has been accepted for inclusion in a future issue of this journal. Content is final as presented, with the exception of pagination.

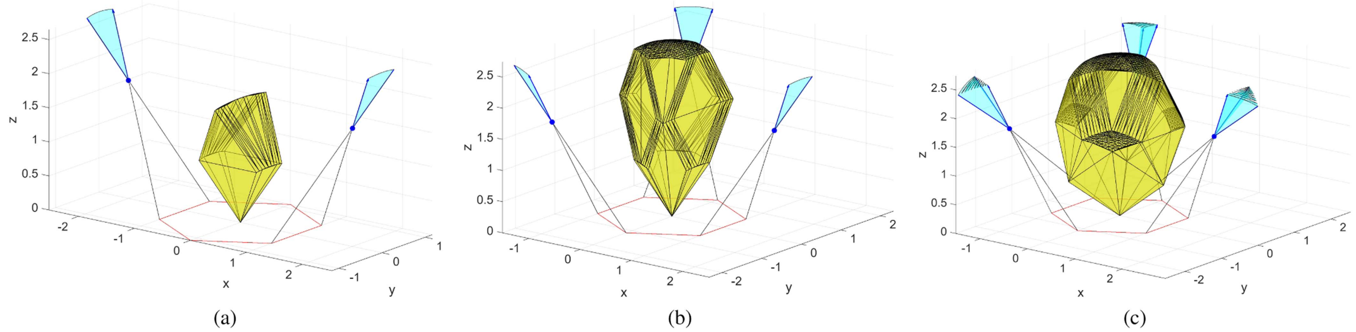

Fig. 4. Grasp Wrench Space and cables cones for three different configurations, considering only the forces. The cyan regions represent the cables cones and the yellow polyhedrons represent all the possible forces that can be applied to the object when the drone forces comply with the cables constraints. (a) 2 drones and 4 cables; (b) 3 drones and 6 cables; (c) 3 drones and 9 cables.

by each drone i, that is

$$\mathcal{W} = \{\mathbf{w} \,|\, \mathbf{w} = \sum_{i=1}^{n_d} \sum_{j=1}^{n_{c_i}} \sigma_{i,j} \mathbf{w}_{ij},\ \|\lambda_i'\| \leq \lambda_{i,\max}'\}. \quad (14)$$

Fig. 4 graphically shows the cables cones and the force components of the Grasp Wrench Space of the configurations taken into account in the representative examples of Section III-B. These plots give a geometric intuition of how the wrench space grows as the number of drones and cables increases.

Remark: Whenever the position of the drone changes w.r.t. the object, the Grasp Matrix must be updated accordingly. This situation is analogous to a case in which a contact point is changed by moving the finger of a multifingered hand while maintaining the grasp. However, while repositioning a finger without loosing the object is, in general, a challenging task, in tethered aerial manipulation, cables allow the drones to keep a secure connection while changing positions without the risk of losing contact. This feature can be exploited to easily reconfigure the system, as also shown in the examples included in the Supplementary Material.

IV. Experimental Validation

A. Objectives

The main objective of the conducted experiments was to validate the model described in this article. Two different experimental scenarios have been considered. In scenario A, the object is fixed w.r.t the world frame $\{\mathbf{N}\}$. In this way, all wrenches measured at the object are generated by the drones, allowing to validate the model limiting dynamic effects and external disturbances. In scenario B, the object is manipulated in its configuration space SE(3) to demonstrate the validity of the model also in free flight motion involving dynamics. For each Scenario, two different configurations of aerial vehicles have been considered: in Experiments A.1 and B.1, we used two drones with two cables for each drone; in Experiments A.2 and B.2, we used three drones with one cable per drone. As shown in Section III, the total number of cables determines the dimension of $\mathcal{N}(\mathbf{G}^{\mathrm{T}})$. Therefore, for both the chosen configurations $\mathcal{N}(\mathbf{G}^{\mathrm{T}})$ are nontrivial: $\mathrm{rank}(\mathbf{N}(\mathbf{G}^{\mathrm{T}})) = 2$ in Experiments A.1 and B.1, $\mathrm{rank}(\mathbf{N}(\mathbf{G}^{\mathrm{T}})) = 3$ in Experiments A.2 and B.2.

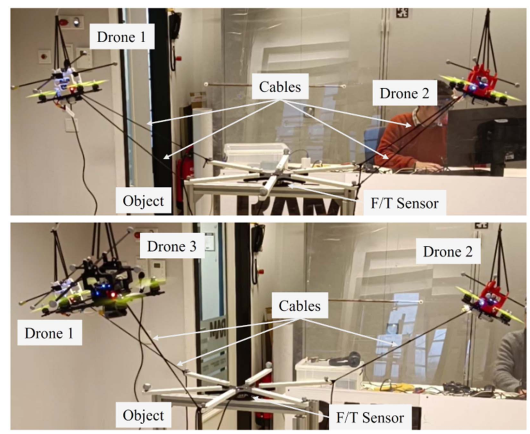

Fig. 5. Scenario A: experimental setup. The object is fixed to a F/T sensor. Top (A.1): two drones, two cables per drone. Bottom (A.2): three drones, one cable per drone. The supporting cables above the drones were used only to hang the drones while they were not flying.

To show the validity of the proposed model, we aimed at verifying that, for all configurations, as long as the cables constraints are satisfied, the following properties hold: 1) the wrenches applied to the object by exerting different drone forces correspond to the ones computed with the model in simulation, 2) the object wrenches belonging to the $\mathcal{N}(\mathbf{G}^{\mathrm{T}})$ are never generated by the dones, and 3) all generated object wrenches belong to the Grasp Wrench Space $\mathcal{W}$.

B. Experimental Setup

The experimental setups for the two scenarios are shown in Figs. 5 and 6. In scenario A, each drone is designed and developed based on a 4-in FPV drone frame mounted by Crazyflie 2.0 flight controller, and has a mass of 0.233 kg. In scenario B, Crazyflie nano quadrotors were used, having a mass of 0.029 kg. In both scenarios, the Crazyswarm software framework is used for data communication, multidrone control, and state estimation [28]. An offboard computer is used to send the reference thrust and attitude to the drones via radio based on the feedback signals, including the drone poses from a motion tracking system (Optitrack, NaturalPoint, Inc.) and the drone attitudes from the

This article has been accepted for inclusion in a future issue of this journal. Content is final as presented, with the exception of pagination.

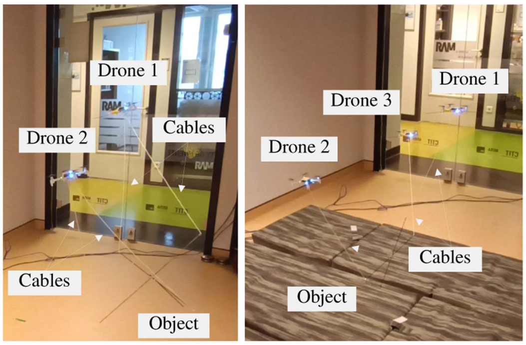

Fig. 6. Scenario B: experimental setup. The drones manipulate the object in free flight. Left (B.1): two drones, two cables per drone. Right (B.2): three drones, one cable per drone.

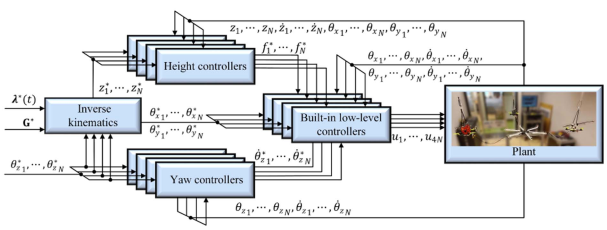

Fig. 7. Scenario A: drones control scheme. The height and attitudinal references for each drone are computed via inverse kinematics with desired Grasp Matrix $\mathbf{G}^*$, wrench λ^*, and drones' yaw angles. Each drone has its own low-level attitude controller, height controller, and yaw controller.

onboard micro control units. Once the drones receive the reference thrust and attitude, the built-in flight attitude controllers generate suitable propeller speeds to track the reference.

In scenario A, to measure the wrench applied by the drones to the object, an ATI mini force/torque (F/T) sensor (ATI Industrial Automation, Inc., USA) is used, and the measurements from the F/T sensor are sent to the offboard computer. In scenario B, a direct measurement of the wrench acting on the object is not available, hence the wrench applied on the object by drones $\mathbf{w} = [\mathbf{f}^{\mathrm{T}}, (\mathbf{R}_{\mathbf{B}}^{\mathbf{N}}\, {}^{B}\tau)^{\mathrm{T}}]^{\mathrm{T}}$ is obtained using the tracking measurements and the object dynamic equations

$$\begin{cases} m_{obj}\ddot{\mathbf{p}} - [0, 0, m_{obj} g_0]^{\mathrm{T}} = \mathbf{f} \\ {}^{B}\mathbf{I}^{B}\dot{\omega} + {}^{B}\omega \times ({}^{B}\mathbf{I}^{B}\omega) = {}^{B}\tau \end{cases} \tag{15}$$

where ${}^{B}\omega = (\mathbf{R}_{\mathbf{B}}^{\mathbf{N}\,\mathrm{T}}\dot{\mathbf{R}}_{\mathbf{B}}^{\mathbf{N}})^{\vee}$ is the angular velocity of the object in $\{\mathbf{B}\}$, $m_{\text{obj}} = 0.005$ kg is the object's mass, and ${}^{B}\mathbf{I}$ is the rotational inertia w.r.t $\{\mathbf{B}\}$. The object's linear acceleration $\ddot{\mathbf{p}}$, angular velocity ${}^{B}\omega$ and angular acceleration ${}^{B}\dot{\omega}$ were obtain via Savitzky–Golay filter.

C. Control of the Drones

In scenario A, the drones were controlled to maintain a fixed position in the space and to apply forces spanning the cables cone in that configuration. In scenario B, dynamic trajectories were assigned to each drone.

In Scenario A, the control structure in Fig. 7 is designed to apply a wrench to the object. The cascaded control structure has two layers: for the inner loop, the built-in low-level controller for each drone receives reference thrust f_i^*, desired roll/pitch angles $\{\theta_{xi}^*, \theta_{yi}^*\}$, desired yaw change rate $\dot{\theta}_{zi}^*$, and generates its own propeller spinning speeds $\{u_{4i-3}, \ldots, u_{4i}\}$, which are the control inputs to the systems. The outer loop is decoupled into drones' height control and yaw control. The inputs of these two subloops are obtained via inverse kinematics calculation, which could be expressed as

$$\begin{cases} \theta_{xi}^* = \arcsin \frac{-[0,1,0]^{\mathrm{T}}\mathbf{H}_i^{\mathrm{T}}\boldsymbol{\lambda}_i}{\cos\theta_{yi}^* \left\|\mathbf{H}_i^{\mathrm{T}}\boldsymbol{\lambda}_i + [0,0,m_i g_0]^{\mathrm{T}}\right\|_2} \\ \theta_{yi}^* = \arcsin \frac{[1,0,0]^{\mathrm{T}}\mathbf{H}_i^{\mathrm{T}}\boldsymbol{\lambda}_i}{\left\|\mathbf{H}_i^{\mathrm{T}}\boldsymbol{\lambda}_i + [0,0,m_i g_0]^{\mathrm{T}}\right\|_2} \\ z_i^* = [0, 0, 1]^{\mathrm{T}}\boldsymbol{c}_i. \end{cases} \tag{16}$$

The yaw feedback loop of each drone employs a standard proportional-derivative (PD) law. For stabilizing the altitude loop, a nonlinear PD law plus feedforward term is implemented

$$f_i^* = \frac{m_i g_0 + k_p(z_i^* - z_i) + k_d(\dot{z}_i^* - \dot{z}_i)}{\cos\theta_{xi}\cos\theta_{yi}} \tag{17}$$

where $k_p = 1.6$ and $k_d = 0.8$ are the proportional and derivative gains, respectively. After that, the thrust magnitude reference is transferred into the thrust command s, a 16-bit (0-65535) type data.

In Scenario B, a standard cascaded position–attitude controller is implemented for each drone to track its reference trajectory [29].

In this work, the relationship between the thrust command and thrust magnitude is obtained from an identification test, in which the thrust magnitude of different drones powered in different battery states is measured with the F/T sensor. Drones were attached to the F/T sensor and thrust magnitudes measurements were gathered. Then, a polynomial-based map between the thrust command and the actual measured thrust magnitude was fitted

$$f_i = p_1\hat{s}^3 + p_2\hat{s}^2 + p_3\hat{s} + p_4 + \Delta f_i \tag{18}$$

where $\hat{s} = s/65535$ is the regularized thrust command, and Δf_i is the thrust magnitude uncertainty. In Scenario A, values were set as $p_1 = -14.45$, $p_2 = 19.61$, $p_3 = 0.1795$, and $p_4 = 0.05925$, and whereas the bound of the actuation uncertainty was estimated as $|\Delta f_i| < 0.6427$ N. In scenario B, $p_1 = -0.1498$, $p_2 = 0.1085$, $p_3 = 0.4082$, and $p_4 = 0.0117$ for drones 1 and 2, and $p_1 = -0.4230$, $p_2 = 0.6042$, $p_3 = 0.2428$, and $p_4 = 0.009$ for drone 3, whereas $|\Delta f_i| < 0.6427$ N.

The uncertainties arising from actuation and sensors in the experimental validation are detailed in Section S.2 of the Supplementary Material.

D. Results

In Figs. 8 and 9, we show how the angle of the applied force and the length of the cables varied throughout Experiments A.1 and B.1. For each drone i, we computed the angles β_i between the cables cones limits (i.e., the imaginary prolongations of the cables), and γ_i between the cables cones limits and λ_i. The two angles are depicted in Fig. 8(a). As shown in Fig. 8(b) and (c) for Experiment A.1, and in Fig. 9(a) and (b) for Experiment B.1,

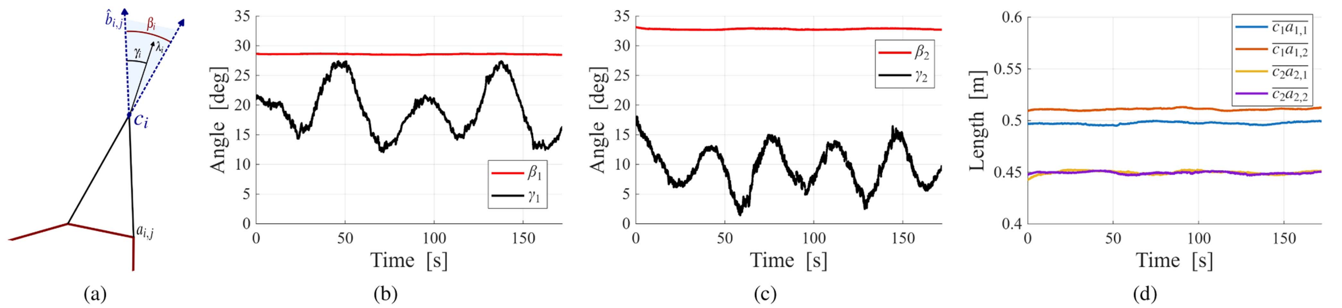

Fig. 8. Cables constraints in Experiment A. (a) Main quantities and notation. (b) and (c) Angles β_i and γ_i for drones 1 and 2, respectively. (d) Length of the cables.

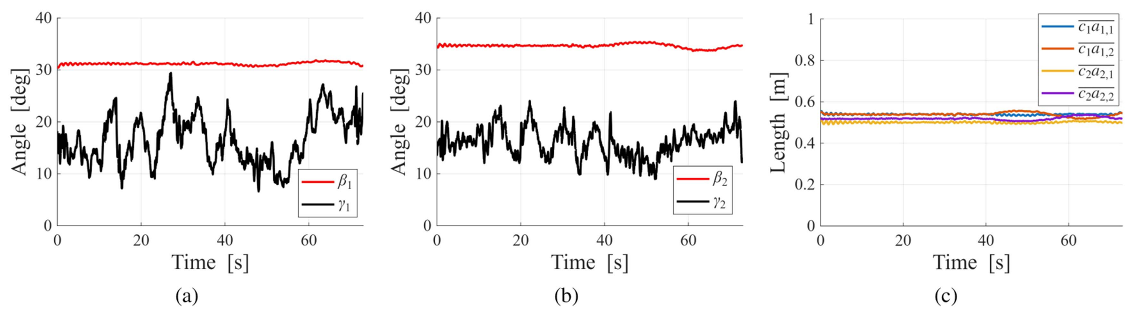

Fig. 9. Cables constraints in Experiment B.1. (a) and (b) Angles β_i and γ_i for drone 1 and drone 2, respectively. (c) Length of the cables.

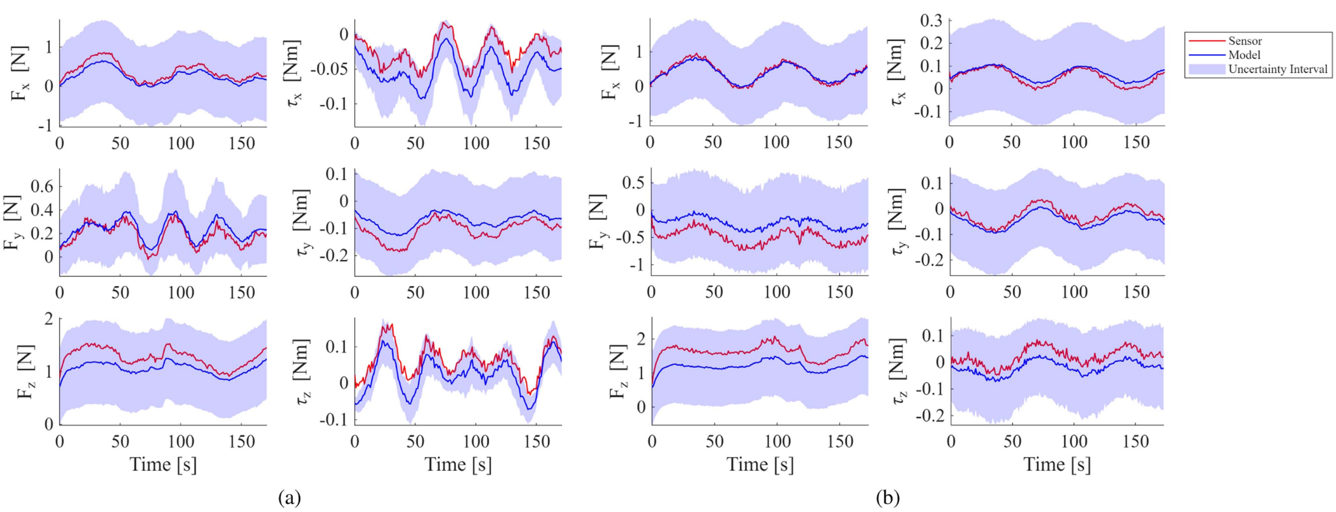

Fig. 10. Scenario A: comparison between the wrench applied on the object measured by the F/T sensor (red) and the one computed using the model (blue) for the two experiments. The violet interval defines the range of uncertainty due to the installation angle of the sensor and the drone thrust commands. (a) Experiment A.1. (b) Experiment A.2.

for both drones γ_i remain between 0 and β_i and hence the cables constraints are satisfied. As a consequence, despite some effects due to the cables elasticity and uncertainties, the cables remain taut during the experiment, as reported in Figs. 8(d) and 9(c). In Experiments A.2 and B.2, where only one cable is attached to each drone, spanning the cables cone only corresponds to changing the intensity of the force component along the cable λ_i, as depicted in Fig. 3. In addition, while with two cables the cables constraints impose that λ_i belongs to the portion of space included between the prolongation of the cables, when only one cable is attached to drone i the cables constraints are satisfied as long as $\lambda_i > 0$.

To analyse the first property listed in Section IV-A, we compared the actual object wrench measured with the F/T sensor and the theoretical value computed using the proposed model. The obtained results are shown in Figs. 10 and 11. In Scenario A, the uncertainty is affected by both the thrust command and the sensor installation angle, whereas in Scenario B only by

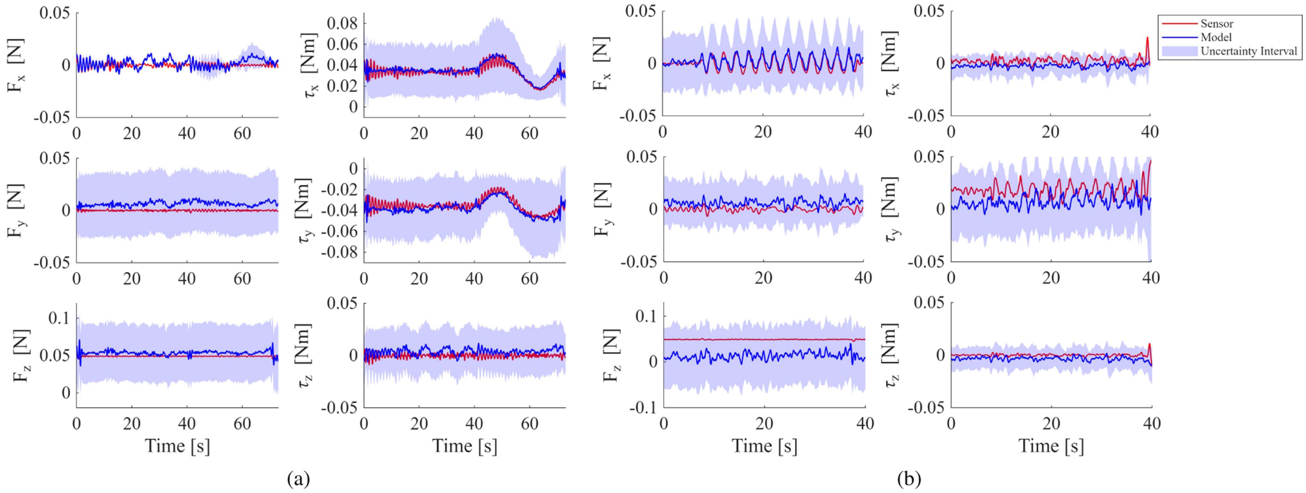

Fig. 11. Scenario B: comparison between the wrench applied on the object computed using the object tracking measurements (red) and the one computed using the model (blue) for the two experiments. The violet interval defines the range of uncertainty due to the drone thrust commands. (a) Experiment B.1. (b) Experiment B.2.

the thrust command. In both experiments, the measured wrench mostly falls within the uncertainty range, thereby validating the proposed model. There are only some small deviations in Experiment A.1, in τ_x and τ_z, and in Experiment B.1 in F_x, due to unmodeled disturbances, including cable elasticity, object structure deformation, tracking errors, and position offset between the cable attachment point on the drone and drone's center of mass.

To assess that each generated wrench $\mathbf{w}$ does not belong to the $\mathcal{N}(\mathbf{G}^{\mathrm{T}})$ (second property listed in Section IV-A), a possible approach is to verify that the matrix $\mathbf{A} = [\mathbf{N}(\hat{\mathbf{G}}^{\mathrm{T}})\ \frac{\hat{\mathbf{w}}}{\|\hat{\mathbf{w}}\|}]$ is full rank. $\hat{\mathbf{G}}$ and $\hat{\mathbf{w}}$ are the scaled grasp matrix $\mathbf{G}$ and scaled wrench $\mathbf{w}$, obtained by dividing their respective torques components by a characteristic length l, chosen as the maximum distance between the drones and the center of mass of the object, to ensure physical consistency, and $\mathbf{N}(\hat{\mathbf{G}}^{\mathrm{T}})$ is an orthonormal basis of $\mathcal{N}(\hat{\mathbf{G}}^{\mathrm{T}})$. The matrix $\mathbf{A}$ was verified to have full rank for each generated object wrench $\mathbf{w}$, inspecting the number of nonzero singular values, given numerical precision. To further show this, we also computed the values of the condition number during the experiments. The condition number of a matrix, defined as the ratio between its maximum and the minimum singular values, provides a measure of how close a matrix is to being singular and, consequently, to losing rank [30]. A low condition number indicates a well-conditioned matrix, whereas a high condition number indicates an ill-conditioned matrix. Typically, the condition number ranges from 1 (for a unitary matrix) to very large values (tending to infinite) for matrices that are nearly singular. In Figs. 12 and 13, the condition number of matrix $\mathbf{A}$ in the two experiments is reported. It always remains bounded and close to 1, confirming that the matrix $\mathbf{A}$ is far from losing rank.

To verify that every generated wrench $\mathbf{w}$ measured by the F/T sensor belonged to the Grasp Wrench Space $\mathcal{W}$ (third property listed in Section IV-A), we computed the minimum distance

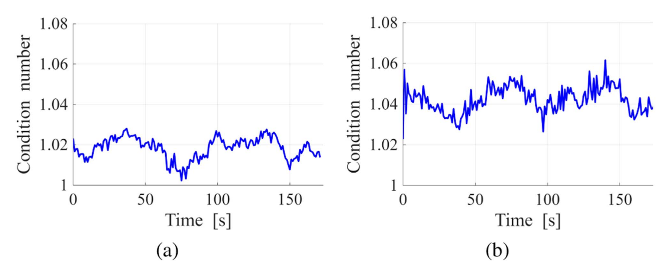

Fig. 12. Scenario A: condition number of matrix $\mathbf{A}$ in the two experiments. (a) Experiment A.1. (b) Experiment A.2.

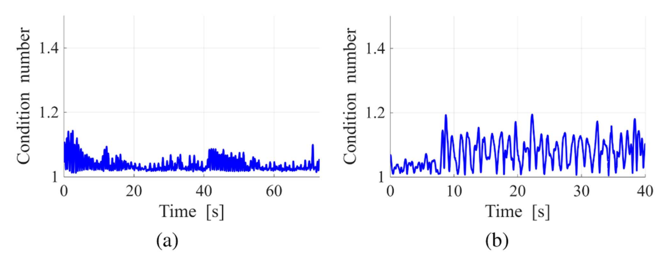

Fig. 13. Scenario B: condition number of matrix $\mathbf{A}$ in the two experiments. (a) Experiment B.1. (b) Experiment B.2.

of the measured wrenches from the boundaries of $\mathcal{W}$. $\mathcal{W}$ was computed considering a drone maximum thrust $\lambda'_{i,\max}$ of 4 N for Scenario A, and of 0.4 N for Scenario B. $\mathcal{W}$ and the measured wrenches were first projected onto the n_c-dimensional space corresponding to the image of $\mathbf{G}$. Then, the minimum distance $d_{\min}$ of each projected wrench $\mathbf{w}_p \in \mathbb{R}^{n_c}$ from the m facets of the projected Grasp Wrench Space is computed as

$$d_{\min} = \min_{j=1,\dots,m} \frac{\langle \mathbf{n}_j, \mathbf{w}_p - \mathbf{p}_j \rangle}{\|\mathbf{n}_j\|} \tag{19}$$

where $\mathbf{n}_j \in \mathbb{R}^{n_c}$ is the normal vector to the jth facet pointing inside the wrench space, $\mathbf{p}_j \in \mathbb{R}^{n_c}$ is a point belonging to the jth

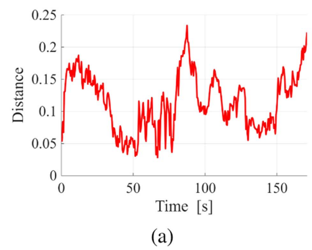

Fig. 14. Scenario A: the minimum distance between the wrenches measured with the F/T sensor and the Grasp Wrench Space limit surfaces. (a) Experiment A.1. (b) Experiment A.2.

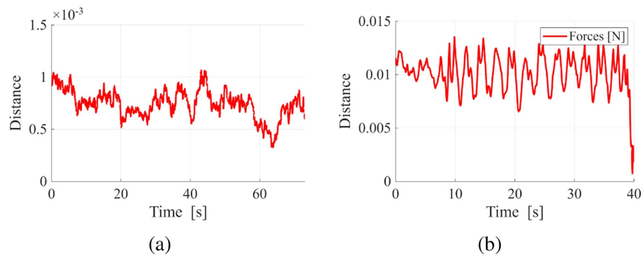

Fig. 15. Scenario B: the minimum distance between the wrenches computed using the object tracking measurements and the Grasp Wrench Space limit surfaces. (a) Experiment B.1. (b) Experiment B.2.

facet, $\|\cdot\|$ is the Euclidean norm, and $\langle\cdot,\cdot\rangle$ is the dot product. The resulting values for the two experiments are reported in Figs. 14 and 15. In both scenarios, the measured wrenches are always contained in the theoretical Grasp Wrench Space, as the distance of the measured wrenches form the wrench space boundaries is always positive.

V. Discussion

The experimental results validate the proposed modeling framework by demonstrating that it accurately captures the wrench applied to the object, and that the grasp-based formulation provides additional value allowing to systematically describe the set of wrenches that can and cannot be resisted, accounting for drone's actuation limits and cables tautness constraints. This is demonstrated across multiple configurations, illustrating the scalability of the proposed formulation, which generalizes to systems with an arbitrary number of drones and cables per drone. Moreover, the proposed framework can be directly used to formulate optimization problems, such as minimizing the total thrust or reducing the likelihood of cable slackening, in analogy with multifinger grasping, as demonstrated in the Supplementary Material.

The developed formulation assumes that the cables considered in the Selection Matrix $\mathbf{H}$ remain taut, which is ensured as long as the transmitted forces satisfy the cables constraints. This assumption has been widely adopted and demonstrated as practically effective in works on tethered aerial manipulation for object pose control [7], [21], [22], [25], [31]. When the drone force approaches the cables cone limits, the cables that are most likely to become slack are those in which the tension is approaching zero. This indicates that these cables are minimally contributing to the wrench applied to the object. Therefore, cables that significantly contribute to the wrench applied on the object are less likely to become slack, while if a cable is near to a zero tension, then it contributes negligibly to the wrench applied to the object.

In the cable-suspended manipulation model, if the force transmitted by a drone λ_i lies outside the corresponding cables cone, the the cables become slack. The slackening of a cable is easily taken into account by the proposed model, thanks to the possibility to modify the Selection Matrix $\mathbf{H}$ to consider that the force component along the cable cannot be transmitted to the object anymore. On the one hand, a slack cable can give more freedom to the drone, enlarging its manipulation capabilities along certain directions. However, the slackening causes the loss of the ability to apply force along the cable. Thus, slackening cables limit the manipulation capabilities of the system, which becomes less capable of rejecting external disturbances. Lastly, in grasping with multifingered hands, when a force is applied outside the friction cone, it leads to the slip of the contact point, and this may result in the object being dropped. Instead, in cable-suspended manipulation, the object is not lost and the tautness of the cable can be regained.

A current limitation is that the proposed formulation assumes inextensible cables. As demonstrated by the experimental evaluation, if the cables present negligible elasticity, then the model accurately describes the force transmission and structural properties of the system. In future work, we plan to investigate the use of elastic cables taking it into account in the model of the system. A possibility is to include in the model the elasticity of the cables based on the concept of compliant grasps [4].

VI. Conclusion

In this work, we propose a mathematical model for cable-suspended multidrone manipulation that is based on the grasp model for multifingered hands developed in literature, detailing the analogies and differences between the two models. The conducted experiments demonstrated the validity of the proposed model for different configurations of drones and cables, opening the possibility of exploiting established tools from robotic grasping for the analysis and control of cable-suspended multidrone systems.

As an example, in future work we will exploit grasp quality measures [32] to reconfigure the drones to maximize resistance to external disturbances, or to optimize the configuration depending on the task objective, identifying the optimal number of cables and drones and the optimal anchor points of the cables on the object.

References

[1] V. Babin and C. Gosselin, "Mechanisms for robotic grasping and manipulation," *Annu. Rev. Control, Robot., Auton. Syst.*, vol. 4, pp. 573–593, 2021.

[2] D. Prattichizzo and J. C. Trinkle, "Grasping," in *Springer Handbook of Robotics*, B. Siciliano and O. Khatib, Eds. Berlin, Germany: Springer, 2016, pp. 955–988.

[3] R. M. Murray, Z. Li, and S. S. Sastry, *A Mathematical Introduction to Robotic Manipulation*. Boca Raton, FL, USA: CRC Press, 2017.

[4] M. Pozzi, M. Malvezzi, and D. Prattichizzo, "On grasp quality measures: Grasp robustness and contact force distribution in underactuated and compliant robotic hands," *IEEE Robot. Automat. Lett.*, vol. 2, no. 1, pp. 329–336, Jan. 2017.

[5] G. Salvietti, M. Malvezzi, G. Gioioso, and D. Prattichizzo, "Modeling compliant grasps exploiting environmental constraints," in *Proc. IEEE Int. Conf. Robot. Automat.*, 2015, pp. 4941–4946.

[6] G. Gioioso, A. Franchi, G. Salvietti, S. Scheggi, and D. Prattichizzo, "The flying hand: A formation of UAVs for cooperative aerial tele-manipulation," in *Proc. IEEE Int. Conf. Robot. Automat.*, 2014, pp. 4335–4341.

[7] D. Sanalitro, H. J. Savino, M. Tognon, J. Cortés, and A. Franchi, "Full-pose manipulation control of a cable-suspended load with multiple UAVs under uncertainties," *IEEE Robot. Automat. Lett.*, vol. 5, no. 2, pp. 2185–2191, Apr. 2020.

[8] I. Ebert-Uphoff and P. A. Voglewede, "On the connections between cable-driven robots, parallel manipulators and grasping," in *Proc. IEEE Int. Conf. Robot. Automat.*, 2004, vol. 5, pp. 4521–4526.

[9] J. Borras and A. M. Dollar, "Framework comparison between a multifingered hand and a parallel manipulator," in *Proc. Comput. Kinematics: Proc. 6th Int. Workshop Comput. Kinematics*, 2014, pp. 219–227.

[10] C. Gabellieri, M. Tognon, D. Sanalitro, and A. Franchi, "Equilibria, stability, and sensitivity for the aerial suspended beam robotic system subject to parameter uncertainty," *IEEE Trans. Robot.*, vol. 39, no. 5, pp. 3977–3993, Oct. 2023.

[11] M. Manubens, D. Devaurs, L. Ros, and J. Cortés, "Motion planning for 6-d manipulation with aerial towed-cable systems," in *Proc. Robot.: Sci. Syst.*, 2013, Art. no. 8p.

[12] J. M. Porta, L. Ros, O. Bohigas, M. Manubens, C. Rosales, and L. Jaillet, "The CUIK suite: Analyzing the motion closed-chain multibody systems," *IEEE Robot. Automat. Mag.*, vol. 21, no. 3, pp. 105–114, Sep. 2014.

[13] B. Siciliano, L. Villani, G. Oriolo, and A. De Luca, "Cooperative Manipulation," *Foundations of Robotics*, Cham: Springer Nature Switzerland, pp. 591–623, 2025.

[14] E. Özgür, G. Gogu, and Y. Mezouar, "A study on dexterous grasps via parallel manipulation analogy," *J. Intell. Robotic Syst.*, vol. 87, no. 1, pp. 3–14, 2017.

[15] J. Borras and A. M. Dollar, "Analyzing dexterous hands using a parallel robots framework," *Auton. Robots*, vol. 36, pp. 169–180, 2014.

[16] P. A. Voglewede and I. Ebert-Uphoff, "Application of the antipodal grasp theorem to cable-driven robots," *IEEE Trans. Robot.*, vol. 21, no. 4, pp. 713–718, Aug. 2005.

[17] P. Bosscher, A. T. Riechel, and I. Ebert-Uphoff, "Wrench-feasible workspace generation for cable-driven robots," *IEEE Trans. Robot.*, vol. 22, no. 5, pp. 890–902, Oct. 2006.

[18] O. Bohigas, M. Manubens, and L. Ros, "Planning wrench-feasible motions for cable-driven hexapods," *IEEE Trans. Robot.*, vol. 32, no. 2, pp. 442–451, Apr. 2016.

[19] G. Cortigiani, M. Malvezzi, D. Prattichizzo, and M. Pozzi, "Human-robot collaborative cable-suspended manipulation with contact distinction," *IEEE Robot. Automat. Lett.*, vol. 10, no. 1, pp. 740–747, Jan. 2025.

[20] A. Ollero, M. Tognon, A. Suarez, D. Lee, and A. Franchi, "Past, present, and future of aerial robotic manipulators," *IEEE Trans. Robot.*, vol. 38, no. 1, pp. 626–645, Feb. 2022.

[21] J. Estevez, G. Garate, J. M. Lopez-Guede, and M. Larrea, "Review of aerial transportation of suspended-cable payloads with quadrotors," *Drones*, vol. 8, no. 2, 2024, Art. no. 35.

[22] S. C. Barakou, C. S. Tzafestas, and K. P. Valavanis, "A survey of modeling and control approaches for cooperative aerial manipulation," in *Proc. Int. Conf. Unmanned Aircr. Syst.*, 2024, pp. 610–617.

[23] N. Michael, J. Fink, and V. Kumar, "Cooperative manipulation and transportation with aerial robots," *Auton. Robots*, vol. 30, pp. 73–86, 2011.

[24] Q. Jiang and V. Kumar, "The inverse kinematics of cooperative transport with multiple aerial robots," *IEEE Trans. Robot.*, vol. 29, no. 1, pp. 136–145, Feb. 2013.

[25] K. Sreenath and V. Kumar, "Dynamics, control and planning for cooperative manipulation of payloads suspended by cables from multiple quadrotor robots," *rn*, vol. 1, no. r2, 2013, Art. no. r3.

[26] C. Masone, H. H. Bülthoff, and P. Stegagno, "Cooperative transportation of a payload using quadrotors: A reconfigurable cable-driven parallel robot," in *Proc. IEEE/RSJ Int. Conf. Intell. Robots Syst.*, 2016, pp. 1623–1630.

[27] A. Bicchi, "On the closure properties of robotic grasping," *Int. J. Robot. Res.*, vol. 14, no. 4, pp. 319–334, 1995.

[28] J. A. Preiss, W. Honig, G. S. Sukhatme, and N. Ayanian, "CrazySwarm: A large nano-quadcopter swarm," in *Proc. IEEE Int. Conf. Robot. Automat.*, IEEE, 2017, pp. 3299–3304, doi: 10.1109/ICRA.2017.7989376,[Online]. Available: https://github.com/USC-ACTLab/crazyswarm

[29] D. Mellinger and V. Kumar, "Minimum snap trajectory generation and control for quadrotors," in *Proc. IEEE Int. Conf. Robot. Automat.*, 2011, pp. 2520–2525.

[30] J. E. Gentle, "Matrix Algebra: Theory, computations and applications in statistics," vol. 10. New York, NY, USA: Springer New York, 2007.

[31] G. Li and G. Loianno, "Nonlinear model predictive control for cooperative transportation and manipulation of cable suspended payloads with multiple quadrotors," in *Proc. IEEE/RSJ Int. Conf. Intell. Robots Syst.*, 2023, pp. 5034–5041.

[32] M. A. Roa and R. Suarez, "Grasp quality measures: Review and performance," *Auton. Robots*, vol. 38, no. 1, pp. 65–88, 2015.

Giovanni Cortigiani (Graduate Student Member, IEEE) received the B.Sc. degree (cum laude) in computer engineering and the M.Sc. degree (*cum laude*) in artificial intelligence and automation engineering in 2020 and 2022, respectively, from the University of Siena, Siena, Italy, where he is currently working toward the Ph.D. degree in engineering and information science with the Department of Information Engineering and Mathematics.

His research interests include human–robot collaboration, manipulation, and grasping.

Yaolei Shen (Graduate Student Member, IEEE) received the B.Eng. and M.Eng. degrees in mechanical engineering from Northwestern Polytechnical University, Xi'an, China, in 2019 and 2022, respectively. He is currently working toward the Ph.D. degree in electrical engineering with the Robotics and Mechatronics Group, University of Twente, Enschede, The Netherlands.

His research interests include modeling and control of aerial robotic manipulation.

Maria Pozzi (Member, IEEE) received the Ph.D. degree in information engineering and science (with Hons.) from the University of Siena (2019).

She is currently a fixed term Assistant Professor with the University of Siena, Siena, Italy.

In 2018, she was the recipient of the RAS Haptics Grant. In 2021, she was selected as an RSS Pioneer and was invited as a Speaker for the IFRR Global Robotics Colloquium on The Future of Robotic Manipulation. She was an Associate Editor for IEEE/RSJ IROS during 2021–2025, *IEEE Robotics and Automation Magazine* during 2023–2025, and IEEE RAL since 2023.

Chiara Gabellieri (Member, IEEE) received the Ph.D. degree in information engineering from the University of Pisa, Pisa, Italy, in 2021.

She is currently an Assistant Professor with the University of Twente, Enschede, The Netherlands. She was the recipient of the Marie Sklodowska-Curie (MSCA) Postdoc Fellowship with the Flyflic project in 2022. She was a Work Package in the European project AeroSTREAM, and is the local PI of the MSCA Staff Exchange project Neutraweed. She has been an Associate Editor for IEEE RAL since 2023 and was an Associate Editor for ICRA 2022–26 and IROS 2023–25.

Monica Malvezzi (Member, IEEE) received the Ph.D. degree in applied mechanics from the University of Bologna, Bologna, Italy, in 2003.

She was PI for the UNISI unit in the H2020 project INBOTS and in the ERASMUS+ project BEREADY. She is currently an Associate Professor with the University of Siena, Siena, Italy. She is the author of several publications in journals, international conferences, and books and is a Member of the editorial/organizing board of international conferences.

Antonio Franchi (Fellow, IEEE) received the Ph.D. degree in system engineering from the Sapienza University of Rome, Rome, Italy, in 2010, and the HDR degree in science from the National Polytechnic Institute of Toulouse, Toulouse, France, in 2016.

Since 2022, he has been a Full Professor of aerial robotics control with the University of Twente, Enschede, The Netherlands, and since 2023, he has been also a Full Professor with the Department of Computer, Control and Management Engineering, Sapienza University of Rome. He coauthored more than 180 publications in peer-reviewed international journals, books, and conferences.

Domenico Prattichizzo (Fellow, IEEE) received the Ph.D. degree in robotics and automation from the University of Pisa, Pisa, Italy, in 1995.

He is currently a Full Professor of robotics with the University of Siena, Siena, Italy. Since 2009, he has been a Senior Scientist with Istituto Italiano di Tecnoloogia, Genova, Genoa, Italy. He was the Coordinator of the FP7 IP project WEARHAP during 2013–2017) and he is the Coordinator of the Horizon Europe project HARIA during 2022–2026. He has authored more than 200 papers and he is the Cofounder of Weart s.r.l., and of the Italian Institute of Robotics and Intelligent Machines.

Open Access funding provided by ‘Universita Degli Studi di Siena’ within the CRUI CARE Agreement